Abbott, R.N. Jr., Bandy, B.R. and Rajkumar, A. 2013. Cenozoic burial metamorphism in eastern Jamaica. *Caribbean Journal of Earth Science*, **46**, 13-30. © Geological Society of Jamaica. Available online 20th July 2013.

Cenozoic burial metamorphism in eastern Jamaica

RICHARD N. ABBOTT, JR.[1], BETSY R. BANDY[2] AND ADRIANNA RAJKUMAR[3]

[1]*Department of Geology, Appalachian State University, Boone, NC 28608. E-mail: abbottrn@appstate.edu*
[2]*Ministry of Science, Technology, Energy and Mining, Kingston, Jamaica. E-mail: bbandy@mstem.gov.jm*
[3]*School of Geosciences, University of Sydney, Sydney, Australia. E-mail: arajkumar09@gmail.com*

ABSTRACT. This research focuses on clasts of volcanic rock in Early Paleocene (c. 65 Ma) conglomerate near the base of the Wagwater Group in eastern Jamaica. Relict augite (Mg#68), plagioclase (An_{60}) and Fe-Ti oxides in the clasts are consistent with basalt. Mineral assemblages, thermodynamic calculations, and stratigraphy define a P-T path for the following paragenesis: (1) During burial, augite was partially to completely replaced by celadonite and chlorite, and expansion fractures were filled by calcite, laumonite and orthoclase (adularia). P-T conditions reached ~258°C, ~1.2 kbars (3.5 km), c. 61 Ma. Cooling began during the deposition of the youngest strata of the Wagwater Group. (2) Plagioclase was partially replaced by heulandite in response to intermittent hydration during continued cooling and burial beneath a thickening limestone platform. P-T conditions approached ~75°C, 2.6-3.1 kbars (7.7-9.3 km), c. 10 Ma. (3) Plagioclase and heulandite were partially replaced by chabazite in response to hydration during final transpressional uplift. The P-T path is interesting because it involves "hot" burial (low dP/dT) and "cool" uplift (high dP/dT). The results contribute to understanding the evolution of the northern margin of the Caribbean plate.

Key words: burial metamorphism, zeolite facies, celadonite, Caribbean, Jamaica.

1. INTRODUCTION

This project was motivated by otherwise anomalously young 50-54 Ma K-Ar ages for biotite in the Cretaceous basement (Westphalia Schist, Lewis et al., 1973), and by indications of elevated temperatures (>200°C, non-detrital, well-crystallized illite+chlorite+albite) in Eocene strata of the Richmond Formation in the upper part of the Wagwater Group (Rajkumar, 2011; Wright and Dickinson, 1972). We hypothesize that older, hence originally deeper, strata in the group would have been exposed to even higher temperatures, outside the range normally associated with diagenesis. Rock samples from the lowest, exposed strata (Early Paleocene) in the group are examined in an effort to characterize P-T conditions near the base of the Wagwater Group during burial and subsequent exhumation. The objective is to relate the changing P-T conditions to the tectonic evolution of the northern margin of the Caribbean plate.

Abbreviations for minerals and mineral components conform to Kretz (1983), as updated by Whitney and Evans (2011). In this convention, abbreviations for minerals are capitalized; abbreviations for components are not capitalized, e.g., "Ab" standards for a plagioclase with "ab" content greater than 90%. K-Ar ages reported from Lewis et al. (1973) are corrected for currently accepted argon decay constants (Steiger and Jäger, 1977). Absolute stratigraphic ages are consistent with the International Commission on Stratigraphy (ICS, Gradstein et al., 2012).

2. GEOLOGY

Jamaica is the third largest of the islands of the Greater Antilles (**Figure 1A**, Puerto Rico, 4th largest, not shown). The island is cut by the E-W trending left-lateral transform system of the Enriquillo-Plantain Garden fault. As such, the island straddles the boundary between the Caribbean plate and the Gonave microplate (**Figure 1A**; and see DeMets and Wiggins-Grandison, 1997).

The basement was formed as part of a Cretaceous (or earlier) volcanic island arc, and consists of a diverse assemblage of unmetamorphosed and metamorphosed volcanic, sedimentary and plutonic rocks (e.g., Robinson, 1994; Mitchell, 2003, 2006). The arc-related rocks are unconformably overlain by Cenozoic strata, the oldest of which are the subject of this paper. The arc-related basement is now exposed in a number of inliers (**Figure 1B**), where locally the younger strata have been eroded away. The largest of the inliers is the Blue Mountain inlier in eastern Jamaica. The unconformity at the base of the Cenozoic strata indicates that the basement was exposed at the surface by the the end of the Cretaceous or by Early Paleocene.

Along the SW margin of the Blue Mountain inlier, greenschist-blueschist facies Mt. Hibernia Schist and amphibolite facies Westphalia Schist (Draper, 1987; Abbott et al., 1996, 2003; Abbott and Bandy, 2008) have most recently been uplifted in response to compression at a prominent right-step

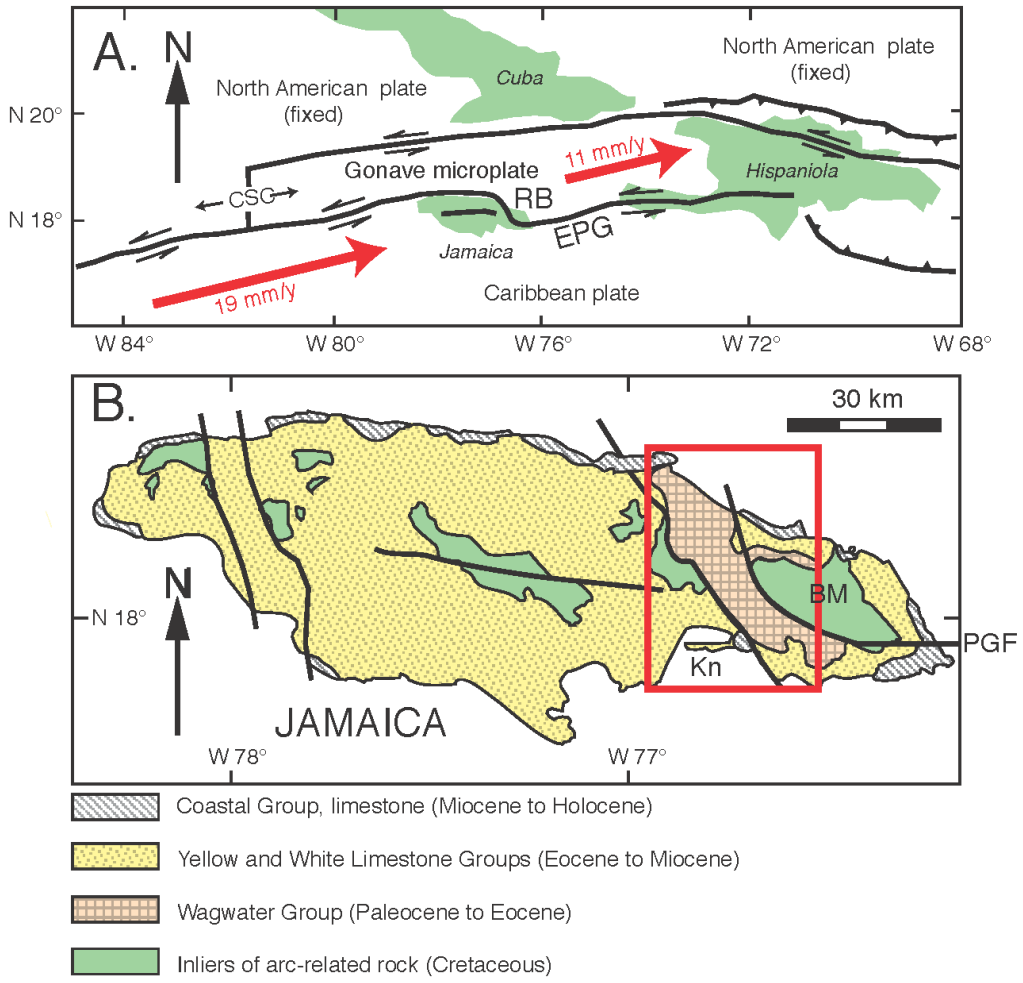

Figure 1. Regional geology. A. Plate tectonic setting of Jamaica. The vectors (DeMets and Wiggins-Grandison, 2007) show the motions of the Caribbean Plate and Gonave microplate relative to the North American Plate. EPG = Enriquillo – Plantain Garden fault, RB = restraining bend, CSC = Cayman spreading center. B. Geologic map of Jamaica, after Mitchell (2013). PGF = Plantain Garden fault, BM = Blue Mountain inlier, Kn = Kingston. Red box is the study area (Figure 2).

restraining bend (Mann et al., 1985; 2007) along the Plantain Garden Fault (**Figure 1A, B**). K-Ar ages on hornblende (Lewis et al., 1973) from the Westphalia Schist give a cooling age of ~77 Ma, while biotite (Lewis et al., 1973) from the same rock gives ages of 50 and 54 Ma. Recently determined whole-rock and K-feldspar $^{40}Ar/^{39}Ar$ cooling ages for Westphalia Schist (**Appendix 1**) are generally consistent with the K-Ar ages. $^{40}Ar/^{39}Ar$ determinations for Westphalia Schist give an Early Eocene whole-rock cooling age of 53 Ma and a Middle Paleocene K-feldspar cooling age of ~60 Ma (**Appendix 1**). The younger ages (50-60 Ma) postdate the unconformity at the base of the Cenozoic strata. This implies a Middle Paleocene—Early Eocene thermal event involving temperatures higher than ~250°C (McDougall and Harrison, 1999; Lovera et al., 2002), that is to say, temperatures sufficiently high to set or reset the K and Ar isotope systems in biotite and K-feldspar. The thermal event may be related to magmatism manifested by volcanic rocks interlayered with Paleocene and Early Eocene sedimentary strata.

The Cenozoic strata (**Figure 2**) reflect three stages in the evolution of the northern edge of the Caribbean Plate (**Figure 3**), here summarized from Robinson (1994), Mann and Burke (1990), and Draper (2008):

(1) Transtensional subsidence: Early Paleocene to Early Eocene redbeds and volcanic rocks of the Wagwater Group occupy a NW-trending half-graben that relates to transtensional tectonics. The group is at least 6.8 km thick (Mann and Burke,

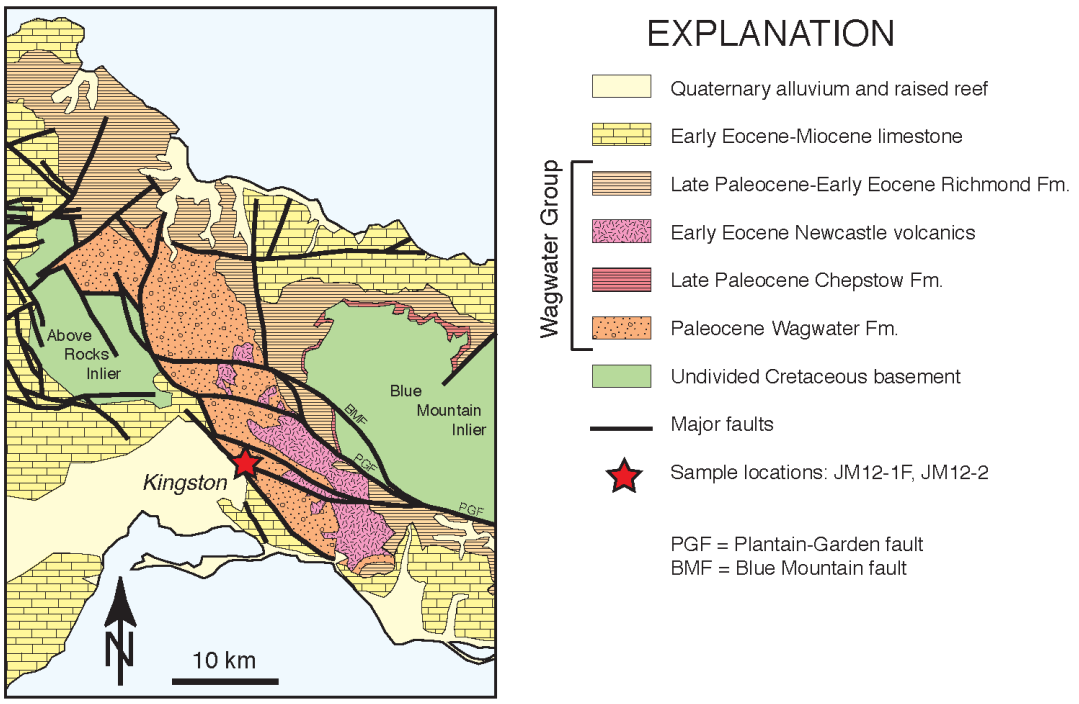

Figure 2. Geologic map of the Wagwater belt and environs, modified from Mann and Burke (1990) with details relating to the distribution of the Richmond Fm. from Pickerill et al. (1992).

1990). East-dipping listric normal faults were active during this time, forming the western margin of the half-graben and affecting the interior of the basin (Draper, 2008).

(2) "Quiescence:" Limestone platform: Middle Eocene to Miocene platform limestone overlies the Wagwater Group and varies in thickness from ~0.9 km (Draper, 2008) to ~2.5 km (Mann and Burke, 1990). The age of the oldest platform limestone varies from Early or Middle Eocene in central Jamaica (Robinson, 1994; Draper, 2008; Mitchell, 2013) to Late Paleocene or Early Eocene in eastern Jamaica (Mann and Burke, 1990; Robinson, 1997). For the purpose of this study, it is assumed that the transition from the Wagwater Group to limestone platform took place in Early Eocene, ~50 Ma (Mann and Burke, 1990, corrected for modern PICKS, Gradstein et al., 2012). The limestone relates to epeirogenic subsidence. Draper (2008) suggested that this subsidence was a result of lithospheric cooling following rifting. There was no active faulting during this time.

(3) Transpressional uplift: Late Miocene (c. 10 Ma, Draper, 2008) to Pleistocene carbonate reef deposits relate to ongoing transpressional uplift. Earlier normal faults (stage 1) were reactivated as reverse faults.

Details of the stratigraphy, pertinent to this study, are reported in **Table 1**. The Wagwater Formation is composed of several distinct members, as defined by Mann and Burke (1990). The Ginger River Member is the oldest unit in the formation. It consists mostly of poorly sorted, dark red to purple, polymict conglomerate, and accounts for most of the stratigraphy of the group. Rock samples used in this study come from boulders in the lowest exposed strata in the Ginger River Member. The sample location is indicated in **Figures 2** and **3**. Other members of the formation include mafic volcanics (Halberstadt Volcanics), felsic volcanics (Newcastle Volcanics), gypsum (Brooks Member), limestone (Woodford Member, Halberstadt Member), thin-bedded sandstone and conglomerate (Pencar River Member), and an upper conglomerate (Dry River Member). The upper conglomerate is distingished from the Ginger River Member stratigraphically and by the presence of clasts of granodiorite. The Richmond Formation is also divided into a number of members. The Roadside Member makes up most of the formation. It consists of thin bedded sandstone, siltstone and shale, in the form of cm- to decimeter-scale turbidite layers. Other members include mafic and felsic volcanics (Nutfield Volcanics), conglomerate (Albany Member), and organic-rich laminate siltstone and mudstone (Langley Member). It is noteworthy that volcanic rocks occur throughout the

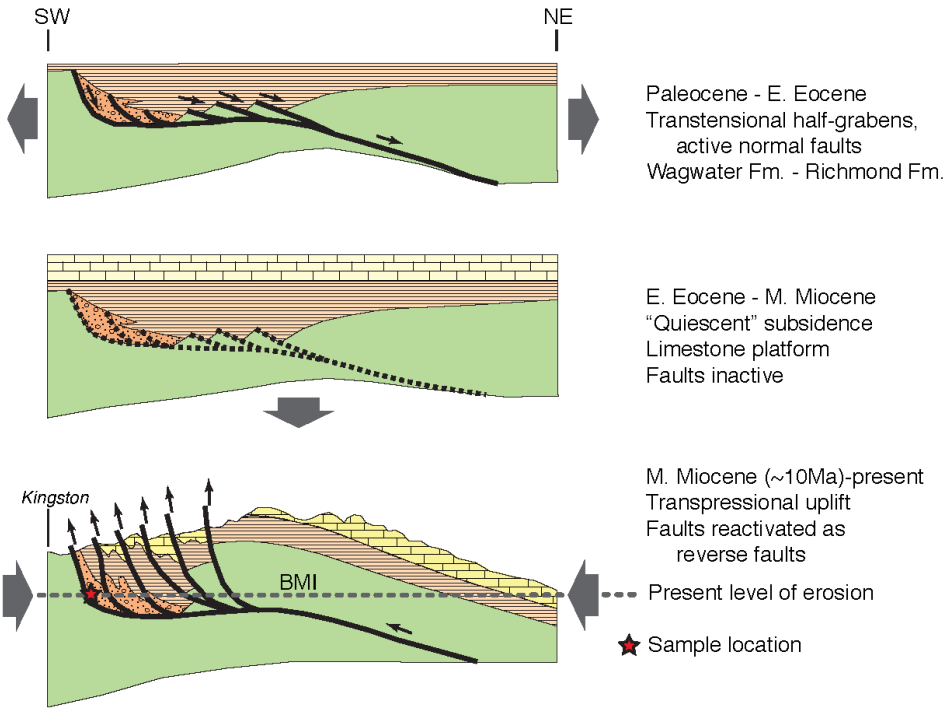

Figure 3. Schematic SW-NE cross sections of the Wagwater Belt, modified from Draper (1998) with profuse apologies. The sequence, from top to bottom, illustrates the three Cenozoic tectonic stages.

Wagwater Group (Mann and Burke, 1990), consistent with the development of a relatively "hot" geothermal gradient (low dP/dT) during transtensional tectonics. The most voluminous expression of volcanism are the Newcastle volcanics (**Figure 2**), which locally separate sedimentary strata of the older Wagwater Formation from sedimentary strata of the younger Richmond Formation (Mann and Burke, 1990). East of the Wagwater Belt (sensu stricto), Paleocene-Eocene sedimentary rocks are referred to as basin flank deposits by Mann and Burke (1990). The oldest of these flank strata is a thin layer of conglomerate that rests nonconformably on metamorphic rocks of the Blue Mountain Inlier. The basal conglomerate is overlain by Paleocene to Early Eocene limestone of the Chepstow Formation (**Figure 2**), which in turn is overlain by undifferentiated turbidites of the Richmond Formation.

3. METHODS

3.1. Sampling.

Collecting suitable samples was informed by the stratigraphy and mapping of Mann and Burke (1990). The lowest exposed strata in the Wagwater Formation (lowest exposed strata in the Ginger River Member) are conveniently accessible on Skyline Drive, near the Kingston community of Papine. Sample JM12-1F was collected at 18°01'11.2" N, 76°44'11.8" W. Sample JM12-2 was collected at 18°01'39.4" N, 76°44'15.6" W (**Figures 2-3**).

3.2. Multivariate analysis.

Multivariate analysis involved three independent variables and five dependent variables. The procedure assumes linear rates of deposition or uplift, and linear rates of heating or cooling in the intervals, 65-61 Ma (lower Wagwater Fm.), 61-56 Ma (upper Wagwater Fm.), 56-50 Ma (Richmond Fm.), 50-10 Ma (limestone) and 10-0 Ma (uplift). The analysis was performed on an Excel spreadsheet, which is available from the first author for the reader's own experimentation.

3.3. X-Ray diffraction.

X-ray diffraction data on powdered whole-rock samples (JM12-1F, JM12-2) were obtained on a Shimazu 6000 X-ray diffractomer (operating conditions: 2Θ 2° – 55° and CuKα radiation). X-ray diffraction data were also determined on vein material separated from the whole rock.

3.4. Energy Dispersive Spectroscopy (EDS).

Chemical analyses of minerals were performed at the College of Arts and Sciences Microscope

Table 1. Stratigraphic data

Stage	Unit	Age at base	thickness	Refs.[a]
(3) Transpression	Coastal Gr.	Late Miocene, c. 10 Ma		3
(2) Quiescence	Platform limestone White limestone Gr. Yellow limestone Gr.	Early Eocene, c. 50 Ma[b]	0.9 to 2.5 km	1,2,3
(1) Transtension	Wagwater Gr.			
	Richmond Fm.	Early Eocene, c. 56 Ma[b]	~1.2 km[c]	1
	Wagwater Fm.	Early Paleocene, c. 65 Ma	>5.6 km[d]	1

[a]References:

1, Mann and Burke (1990, Figure 8, and accompanying discussion)

2, Robinson (1994)

3, Draper (2008, Table, and accompanying discussion)

[b]Age corrected for modern PICKS (Gradstein et al., 2012)

[c]Thickness does not include Chepstow limestone Fm.

[d]Thickness includes the Newcastle volcanics.

Facility, Appalachian State University. The instrument is an FEI Quanta 200 scanning electron microscope, fitted with an EDS microanalyzer (EDAX). Mineral standards were obtained from the Smithsonian Institute (USNM series). Instrument settings were 35 Kv acceleration voltage, 4 μm spot size, 50 s counting time. Raw data were processed with Genesis 3.5 software. The Genesis software has certain peculiarities regarding constraints on the ZAF algorithm. The software does not allow for using more than one standard at a time, and the sum of the weight percents of oxide components is constrained to a user specified value. For the purpose of major oxide analyses, except K_2O, these peculiarities were accommodated satisfactorily by choice of a suitable standard, and by paying special attention to stoichiometry (especially, atomic proportions of cations). For the silicate minerals, USNM omphacite standard (#1106067) was used. For each mineral, the sum of the weight percents of the oxide components was normalized to 100. The low K_2O in the omphacite standard (0.15 wt.%) makes it unreliable for K_2O in silicate minerals with appreciable K_2O (>1 wt.%). In order to accommodate the problem, in each EDS session the USNM microcline standard (#1143966, 15.14 wt.% K_2O) was analyzed as an unknown at the beginning of the session (5 or 6 spots) and at the end of the session (5 or 6 spots). New correction factors were calculated for the major oxides in the microcline standard (Na_2O, K_2O, Al_2O_3, SiO_2). The new correction factors were then applied, in a fashion consistent with ZAF correction procedures, to mineral analyses referred to the omphacite standard (USNM #1106067). The analyses were then renormalized to 100 wt. %. Systematics of the cation proportions (i.e., stoichiometry) indicate that the procedure is successful within expected limits of analytical uncertainty for EDS. For the purpose of comparison with analyses in the literature, and proper identification, analyses for zeolite minerals were re-normalized for expected wt. % of H_2O. Given strict constraints on cation proportions in celadonite and chlorite, and confidence in their proper identification by optical properties and XRD, renormalization of the analyses to an expected wt. % H_2O was not deemed necessary for these minerals. For the Fe-Ti oxide minerals, one standard was used, USNM ilmenite (#96189).

3.5. Thermodynamic calculations.

Thermodynamic calculation were performed using the software THERMOCALC, v. tc325, data set 5.5, 12 November 2004 (Holland and Powell, 1998; Powell et al., 1998; Powell, 2005). Activities of mineral components were calculated using the companion software AX (Holland and Powell, 2000).

4. MINIMUM DEPTH TO THE BASE OF THE WAGWATER FORMATION

Figure 4 is a graph of depth versus time for the oldest exposed strata of the Wagwater Formation (Ginger Ridge Member), the base of the Richmond Formation, and the base of the limestone platform. Deposition commenced at ~65 Ma. Uplift commenced in Late Miocene time, ~10 Ma (Draper, 2008) and continues today. The depths in **Figure 4**

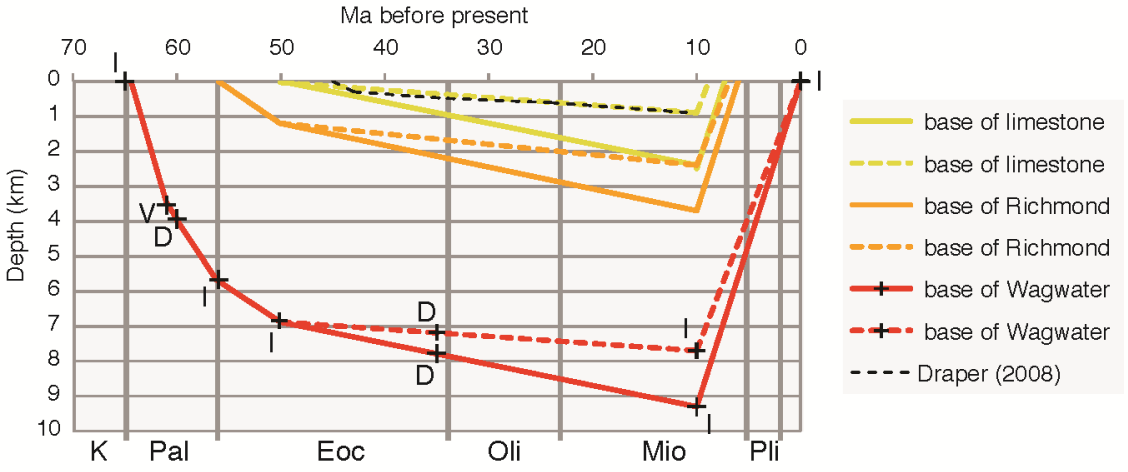

Figure 4. Depth to the oldest exposed strata of the Wagwater Group as a function of time, compiled from Mann and Burke (1990), Robinson (1994) and Draper (2008). The figure also shows the depth to the base of the Richmond Fm. and the depth to the base of the limestone platform (Yellow limestone). In the multivariate model, the age at each control point (+) is invariant. At the control points marked "I" the depth is invariant, at the control point marked "V" the depth is variable, and at the control points marked "D" the depth is dependent. The first interval (65-61 Ma, I-V) relates to the lower Wagwater Formation, the second interval (61-56 Ma, V-D-I) relates to the upper Wagwater Formation, the third interval (56-50 Ma, I-I) relates to the Richmond Formation, the fourth interval (50-10 Ma, I-D-I) relates to deposition of the limestone platform, and the fifth and final interval (10-0 Ma, I-I) relates to ongoing uplift.

serve as the best proxy for pressure, assuming here that 3 km thickness of strata translates to approximately 1 kbar of pressure (3 km ~ 1 kbar).

Control points in **Figure 4** (marked by the crosses, +), refer to the depth (km) to the oldest exposed strata of the Wagwater Formation. Because the base is not exposed at the surface, the control points relate to the minimum depth to the base of the Wagwater Formation, except of course for the first control point, which corresponds to the beginning of deposition. The boundary conditions are:

(1) beginning of deposition (~65 Ma, 0 km), and

(2) present (0 Ma, 0 km).

Four of the control points relate to the cummulative thicknesses in Table 1:

(3) end of deposition of Wagwater Fm./beginning of deposition of Richmond Fm. (~56 Ma, 5.6 km),

(4) end of deposition of Richmond Fm./beginning of deposition of limestone (~50 Ma, 6.8 km),

(5) end of deposition of limestone/beginning of uplift (~10 Ma, 7.7 km, Draper, 2008), and

(6) end of deposition of limestone/beginning of uplift (~10 Ma, 9.3 km, Mann and Burke, 1990).

Four other control points relate to multivariate analysis:

(7) (61 Ma, 3.2-3.8 km; favored depth, 3.5 km),

(8) (60 Ma, 3.9 km, relates to 3.5 km at 61 Ma),

(9) (35 Ma, 7.2 km, Draper, 2008), and

(10) (35 Ma, 7.7 km, Mann and Burke, 1990).

In the multivariate model, the ages at these control points are invariant. The depth at 61 Ma (7) is an independent variable. Reasonable multivariate solutions can be found for depths from 3.2 to 3.8 km. The favored depth at 61 Ma (7) is 3.5 km. The depths at 60 Ma and 35 Ma (9, 10) are dependent variables. The 60-Ma control point corresponds to the Ar-release age for the most retentive sites (>250°C) in K-feldspar (**Appendix 1**). The 35-Ma control points correspond to the Ar-release age for the least retentive sites (~150°C) in K-feldspar (Appendix). In Figure 4, the control point (35 Ma, 7.2 km) is linearly contrained between (~50 Ma, 6.8 km) and (~10 Ma, 7.7 km). Likewise, the control point (35 Ma, 7.7 km) is linearly constrained between (~50 Ma, 6.8 km) and (~10 Ma, 9.3 km). Adjusting the independent variable (7) within reasonable limits does not significantly alter the relationships in **Figure 4**. For comparison, detailed non-linear depth-time data from Draper (2008) are also plotted for the deposition of the limestone platform.

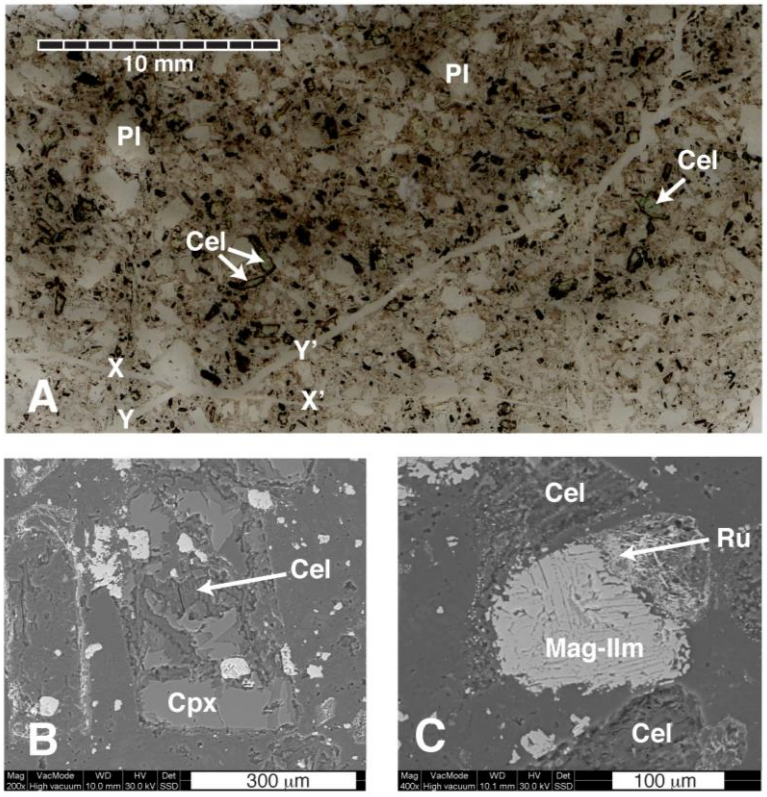

Figure 5. Petrography of sample JM12-1F. A. Digital image of a thin section in plane-polarized light. Three celadonite pseudomorphs after augite are indicated. Euhedral phenocrysts of plagioclase are partially to extensively replaced by heulandite and chabazite. Most of the opaque grains are symplectic intergrowths of magnetite and ilmenite. Most of the matrix has been silicified to quartz and albite. Calcite and minute grains of hematite are ubiquitous. The fractures are filled with calcite, laumontite and orthoclase. Note that plagioclase phenocrysts cut by the fractures show no vein-parallel displacement. All of the fractures are dilational. The apparent displacement on the fine fracture (X-X') near the bottom of the image is an artefact of the opening of the wider diagonal fracture (Y-Y') for a short distance along the preexisting X-X' fracture. B. SEM image of a partial pseudomorph of euhedral phenocrysts of augite (Cpx). The replacement minerals are celadonite, quartz, albite and minor amount of chlorite. The bright grains are symplectic intergrowths of ilmenite and titanomagnetite. C. SEM image of the symplectic intergrowth of ilmenite and titanomagnetite. Aggregates of fine grained rutile appear locally to replace the titanomagnetite-ilmenite grains. Celadonite pseudomorphs after augite are also indicated.

5. PETROGRAPHY

Rock samples (JM12-1F and JM12-2) were chipped from the interiors of boulders in conglomerate near the base of the Wagwater Formation (Ginger River Member). Where sampled, the rock is essentially a monomict boulder conglomerate of well-rounded clasts up to 50 cm. The matrix consists of finer grained lithic clasts of the same petrography as the boulders. In hand specimen, the clasts consist of intermediate purple-grey porphyritic volcanic rock. Phenocrysts of euhedral plagioclase, up to 2 mm, are set in a deep purple aphanitic matrix. The rock has sub-mm-scale fractures filled with white to pink material, most of which is calcite. Where they can be traced with confidence, the fractures extend into the matrix. In thin section (**Figure 5A**), the phenocrysts of plagioclases are well twinned, but the twinning is interrupted by a profusion of irregular μm-scale patches of a low-birefringence silicate, which turns out to to be heulandite (see below). The phenocrysts have narrow, μm-scale discontinuous rims of another low-birefringence silicate, which turns out to be chabazite (see below). Partially to completely pseudomorphed, sub-mm, euhedral phenocrysts of augite are typically rimmed by black, amorphous material, presumed to consist of weathering products, including clay minerals and hematite. Because it is very efficiently removed in the preparation of a polished surface, the amorphous black material could not be properly charactered by

Table 2. Chemical analyses of relict plagioclase and augite

	Plagioclase			Augite	
Samples	JM12-1F, JM12-2			JM12-1F, JM12-2	
no. of analyses	8			7	
	Wt.%	St.Dev.		Wt.%	St.Dev.
Na_2O	4.77	0.44		0.85	0.31
MgO	0.43	0.36		12.44	0.31
Al_2O_3	28.09	0.33		2.09	0.15
SiO_2	53.43	0.45		51.52	1.10
K_2O	0.17	0.11		0.02	0.03
CaO	12.12	0.71		22.59	1.98
TiO_2	0.10	0.04		0.25	0.09
MnO	0.05	0.01		0.23	0.04
FeO	0.84	0.10		9.99	0.69
Total	100.00			100.00	
	Cations pfu[a]	St.Dev.		Cations pfu	St.Dev.
no. oxygen	8			6	
Na	0.43	0.04		0.06	0.02
Mg	0.03	0.02		0.69	0.02
Al	1.53	0.02		0.09	0.01
Si	2.47	0.02		1.92	0.04
K	0.01	0.01		0.00	0.00
Ca	0.60	0.03		0.90	0.08
Ti	0.00	0.00		0.01	0.00
Mn	0.00	0.00		0.01	0.00
Fe	0.03	0.00		0.31	0.02
an ~ Ca/(Ca+Na+K	0.58		wo ~ Ca/2	0.45	
an ~ Al-1 ~ 3-Si	0.53		en ~ Mg/2	0.35	
ab ~ Na/(Ca+Na+K	0.41		fs ~ Fe/2	0.16	
or ~ K/(Ca+Na+K)	0.01				
[a]pfu = per formula unit					

SEM. Bright green celadonite (**Figure 5A**) is the most conspicuous of the minerals that replace the original augite. XRD experiments on powdered whole rock samples confirm the abundant minerals, which include more than one type or composition of plagioclase, quartz, a 10-Å phyllosilicate (celadonite), a 14-Å phyllosilicate (chlorite) and calcite. Plagioclase phenocrysts and other mineral grains that were intersected by the fractures show no fracture-parallel displacement (**Figure 5A**). This means that the fractures are purely dilational, consistent with a transtensional tectonic environment. Other than calcite, the fractures contain euhedral microcrystals of low-birefringence silicate minerals. XRD data on powdered samples of the material filling the fractures confirm that the silicate minerals are laumonite and orthoclase. **Figure 5B** is an SEM image of a partial pseudomorph of augite. Celadonite typically accounts for most of the pseudomorphous minerals. Other minerals, identified by EDS, that make up the pseudomorphs include minor amounts of albite, quartz, chlorite, titanite and calcite. The bright grains are Fe-Ti oxide minerals. **Figure 5C** is an SEM image of a grain of Fe-Ti oxide. The grain consists of a symplectic intergrowth of titanomagnetite (bright) and ilmenite (light grey lamellae). An aggregate of microlaths of rutile occupies an embayment in the symplectite.

Plagioclase and augite in phenocrysts are considered to be primary volcanic minerals. The Fe-Ti oxide grains may also be primary, but the symplectic intergrowth of ilmenite and titanomagnetite suggest subsolidus re-equilibration in response to post-volcanic cooling, unrelated to diagenesis or burial metamorphism. In the present context, titanomagnetite and ilmenite would be protolith minerals. The order of appearance of the key minerals is as follows, inferred from textural relationships:

(1) Protolith minerals (plagioclase, augite, symplectic Fe-Ti oxide).

(2) Minerals pseudomorphous after augite (mainly celadonite, chlorite, albite), and rutile coexisting with titanomagnetite and ilmenite.

(3) Minerals in the fractures (laumontite, orthoclase, calcite).

(4) Heulandite and chabazite.

6. MINERAL CHEMISTRY

6.1. Primary silicate minerals

Average compositions of relict plagioclase and augite are presented in **Table 2**. Observations of extinction angles in cross-polarized light indicate that the plagioclase phenocrysts are not strongly zoned. This is consistent with the low standard deviations for the weight percent oxides and the cations in the average formula unit. Given the relatively high analytical uncertainty in analyses for Na_2O, compared to the other oxide components, the chemical formula was normalized to four tetrahedral cations pfu, i.e., Si+Al = 4. On this basis, the an-content can be calculated in two ways an~Ca/(Ca+Na+K) or an~Al-1(**Table 2**). For either way of estimating an-content, the composition is consistent with laboradorite ($an_{53}ab_{41}or_{01}$ or $an_{58}ab_{41}or_{01}$). The average composition of the relict augite is typical for augite. The small standard deviations indicate that the augite is fairly uniform in composition. The Mg# is 70. While the texture and color of the rock might otherwise suggest an

Table 3. Chemical analyses of celadonite and chlorite

	Celadonite			Celadonite			Chlorite	
Sample	JM12-1F			JM12-2			JM12-1F	
no. of analyses	6			12			10	
	Wt.%	St.Dev.		Wt.%	St.Dev.		Wt.%	St.Dev.
Na_2O	0.44	0.29		0.41	0.21		0.84	0.11
MgO	5.99	1.26		7.27	0.35		25.71	3.28
Al_2O_3	9.12	1.69		7.46	0.94		18.04	1.53
SiO_2	56.68	1.09		56.71	0.66		41.28	4.14
K_2O	9.10	0.39		10.28	0.35		0.11	0.09
CaO	0.71	0.30		0.32	0.09		1.25	0.20
TiO_2	0.24	0.10		0.15	0.08		0.28	0.18
MnO	0.10	0.03		0.15	0.03		0.25	0.07
FeO	17.61	2.13		17.25	0.89		12.24	7.49
Total	100.00			100.00			100.00	
	Cations pfu[a,b]	St.Dev.		Cations pfu	St.Dev.		Cations pfu[c]	St.Dev.
Tetrahedral								
Si	3.72	0.11		3.74	0.05		3.50	0.23
Al	0.28	0.05		0.26	0.03		0.50	0.02
Octahedral								
Al	0.43	0.07		0.32	0.04		1.28	0.06
Mg	0.59	0.12		0.71	0.03		3.24	0.33
Ti	0.01	0.00		0.01	0.00		0.02	0.01
Mn	0.01	0.00		0.01	0.00		0.02	0.00
Fe	0.97	0.13		0.95	0.06		0.86	0.61
[ ][d]	1.00			1.00			0.59	
Interlayer, A								
Na	0.06	0.04		0.05	0.03		0.13	0.02
K	0.76	0.04		0.86	0.04		0.01	0.01
Ca	0.05	0.0202		0.02	0.01		0.11	0.02
[ ]	0.13			0.06			0.74	

[a]pfu = per formula unit
[b]Celadonite (dioctahedral), formula assumes 4 tetrahedral sites pfu, 2 of 3 octahedral sites occupied pfu.
[c]Chlorite, formula assumes 4 tetrahedral sites pfu, 6 octahedral sites pfu, all Fe is Fe^{2+}, Q = 28 (sum cation charges, excluding H^+), Ca+K+Na are in interlayer sites.
[d][ ] = vacancy

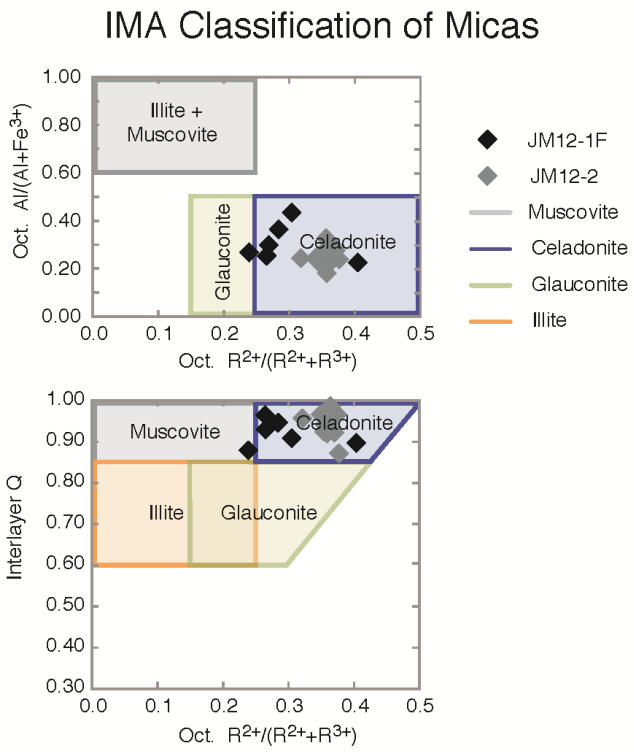

Figure 6. Celadonite analyses from samples JM12-1F (n=6, average composition in Table 3) and JM12-2 (n=12) plotted on classification diagrams for dioctahedral micas (CNMMN, 1998).

andesitic protolith, the composition of the plagioclase and augite are more consistent with a basaltic protolith. This would align the source of the boulders with the earliest manifestations of the Halberstadt volcanics from lower in the strata of the Wagwater Formation.

6.2. Phyllosilicates

The predominant phyllosilicates are celadonite and chlorite. Average compositions are reported in **Table 3**. They occur mainly as pseudomorphs after augite. **Figure 6** shows individual compositions of celadonite plotted in CNMMN (1998) classification diagrams. The composition of chlorite is consistent with penninite (Deer et al., 1973) and is otherwise unremarkable for low-grade metamorphism. The relatively coarse grain size (up to ~0.5 mm), sharp, well-defined XRD peaks, and the compositions of celadonite and chlorite reflect conditions exceeding those normally associated with diagenesis (Coombs et al., 1959; Miyashiro and Shido, 1970; Miyashiro, 1973; Utada, 2001).

6.3. Zeolites, albite, orthoclase

Average compositions for laumontite, heulandite, chabazite, orthoclase and albite are reported in **Table 4**. Classification of the zeolites is consistent with CNMMN (1997) guidelines. While laumontite and heulandite were verified by XRD, chabazite was inferred from the chemical analyses. Representative zeolite compositions from Deer et al. (1973) are reported for comparison. The weight percent analyses determined in this study were normalized for the same amount of H_2O as in the comparison analyses. The standard deviations of the weight percents of the principal oxide components (or corresponding cations pfu) indicate

Table 4. Chemical analyses of zeolites, albite, orthoclase, sample JM12-1F

	Laumontite		DHZ[a] #8		Heulandite		DHZ #5		Chabazite		DHZ #7
no. of analyses	7				7				8		
	Wt.%	St.Dev.	Wt.%		Wt.%	St.Dev.	Wt.%		Wt.%	St.Dev.	Wt.%
Na_2O	0.15	0.19	0.40		0.36	0.38	2.95		0.12	0.19	0.98
MgO	0.23	0.50	bd[b]		0.24	0.30	bd		0.22	0.50	bd
Al_2O_3	21.37	0.59	22.53		16.95	0.22	17.76		18.39	0.59	18.04
SiO_2	50.79	0.80	50.70		56.84	0.54	57.28		47.50	0.80	48.78
K_2O	0.14	0.35	0.30		0.12	0.03	bd		1.40	0.35	0.60
CaO	12.66	0.31	11.54		8.64	0.53	7.18		9.86	0.31	9.77
TiO_2	0.06	0.07	na[b]		1.18	0.22	na		0.11	0.07	na
MnO	0.05	0.03	na		0.06	0.03	na		0.05	0.03	na
FeO	0.17	0.12	0.04		0.22	0.08	bd		0.34	0.12	tr[b]
H_2O[c]	14.40		14.40		15.40		15.40		22.00		22.00
Total	100.00		99.91		100.00		100.57		100.00		100.17
	Cations pfu[d]	St.Dev.			Cations pfu	St.Dev.			Cations pfu	St.Dev.	
Al+Si pfu	24				36				36		
Na	0.09	0.15	0.24		0.33	0.35	2.63		0.12	0.20	0.97
Mg	0.11	0.16	0.01		0.17	0.21	bd		0.17	0.39	bd
Al	7.96	0.16	8.27		9.36	0.12	9.63		11.28	0.37	10.84
Si	16.04	0.16	15.78		26.64	0.12	26.35		24.72	0.37	24.86
K	0.06	0.02	0.12		0.07	0.02	bd		0.93	0.23	0.39
Ca	4.29	0.36	3.85		4.34	0.29	3.54		5.50	0.17	5.34
Ti	0.02	0.01	na		0.42	0.08	na		0.04	0.03	na
Mn	0.01	0.01	na		0.03	0.01	na		0.02	0.01	na
Fe	0.04	0.03	0.01		0.09	0.03	bd		0.15	0.05	tr

	Albite			Orthoclase	
no. of analyses	2			4	
	Wt.%	St.Dev.		Wt.%	St.Dev.
Na_2O	11.19	0.19		0.53	0.42
MgO	0.31	0.43		0.39	0.45
Al_2O_3	20.55	0.01		18.44	0.25
SiO_2	65.70	0.52		62.75	0.75
K_2O	0.11	0.07		16.22	0.29
CaO	1.04	0.64		0.58	0.08
TiO_2	0.14	0.03		0.84	0.19
MnO	0.05	0.01		0.05	0.03
FeO	0.92	0.69		0.21	0.06
Total	100.00			100.00	
	Cations pfu	St.Dev.		Cations pfu	St.Dev.
Al+Si	4.00			4.00	
Na	0.96	0.02		0.05	0.04
Mg	0.02	0.03		0.03	0.03
Al	1.08	0.01		1.03	0.02
Si	2.92	0.01		2.97	0.02
K	0.01	0.00		0.98	0.01
Ca	0.05	0.03		0.03	0.00
Ti	0.00	0.00		0.03	0.01
Mn	0.00	0.00		0.00	0.00
Fe	0.03	0.03		0.01	0.00
an ~ Ca/(Ca+Na+K	0.05			0.03	
an ~ Al-1 ~ 3-Si	0.08			0.03	
or ~ K/(Ca+Na+K)	0.01			0.93	
ab ~ Na/(Ca+Na+K	0.95			0.05	

[a]DHZ = Deer, Howie and Zussman (1985, 15th printing)

[b]bd = below detection, na = not analyzed, tr = trace.

[c]H_2O assumed for zeolites analyzed in this study; measured H_2O for DHZ analyses.

[d]pfu = per formula unit

that each of the zeolite minerals varies little in composition. The average compositions of albite and orthoclase (**Table 4**) show no noteworthy irregularities.

6.4. Fe-Ti oxides

Average compositions for titanomagnetite and ilmenite are reported in **Table 5**. Individual compositions are portrayed in **Figure 7**, which shows relatively small variability in the composition of either mineral. Locally, the minerals coexist with rutile.

7. PHASE RELATIONSHIPS AND TERMODYNAMIC CALCULATIONS

Figure 8 portrays relevant phase relationships involving zeolite minerals, THERMOCALC results relating to the stability of celadonite and the Fe-Ti oxides, and Ar blocking temperatures (**Appendix 1**).

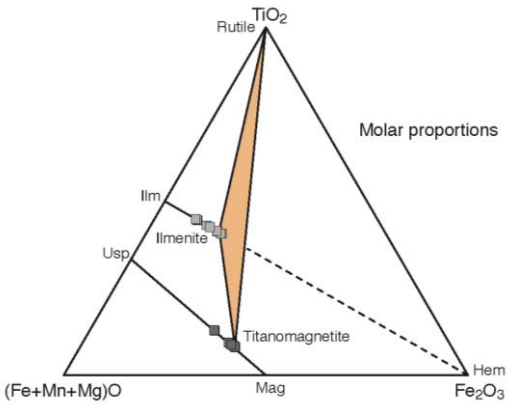

Figure 7. Analyses of ilmenite and titanomagnetite from sample JM12-1F. The ilmenite and titanomagnetite coexist with rutile.

Table 5. Chemical analyses of Fe-Ti oxides, sample JM12-1F

	Magnetite				Ilmenite	
no. of analyses	15				9	
	Wt.%	St.Dev.			Wt.%	St.Dev
MgO	2.83	0.50			2.77	0.58
TiO_2	7.73	1.37			40.68	2.95
MnO	0.77	0.23			0.44	0.11
FeO[a]	88.67	0.97			56.11	3.43
Total	100.00				100.00	
	Cations pfu[b]	St.Dev.			Cations pfu	St.Dev.
Mg+Ti+Mn+Fe	3				2	
Mg	0.15	0.03			0.10	0.02
Ti	0.20	0.04			0.75	0.05
Mn	0.02	0.01			0.01	0.00
Fe	2.62	0.02			1.14	0.07
no. "O" pfu	4				3	
[c]Q	6.41	0.08			5.49	0.11
[c]Fe^{3+}	1.59	0.08			0.51	0.11
[c]Fe^{2+}	1.03	0.06			0.64	0.04
Fe_3O_4 (mag)	0.80	0.04		Fe_2O_3 (hem)	0.25	0.05
Fe_2TiO_4 (usp)	0.12	0.05		$FeTiO_3$ (ilm)	0.64	0.04
Mn_2TiO_4	0.01	0.00		$MnTiO_3$	0.01	0.00
Mg_2TiO_4	0.08	0.01		$MgTiO_3$	0.10	0.02
[a]All Fe reported as FeO						
[b]pfu = per formula unit						
[c]Q = sum of cation charges, assuming all Fe is 2+						
For magnetite, Fe^{3+} = 8-Q, Fe^{2+} = Fe_{total} - Fe^{3+}						
For ilmenite, Fe^{3+} = 6-Q, Fe^{2+} = Fe_{total} - Fe^{3+}						

7.1. Zeolites phase relationships

Phase relationships for the stilbite, heulandite, laumontite and wairikite are from experiments in the CASH system (Cho et al., 1987). The chabazite-stilbite reaction is from Chipera and Apps (2001). Each of the zeolite reactions is terminal to the zeolite on the low-temperature side of the reaction, such that each of the reactions takes one of two general forms:

$$Zeo_{low\text{-}T} \Rightarrow Zeo_{high\text{-}T} + nH_2O, \text{ or}$$

$$Zeo_{low\text{-}T} \Rightarrow Zeo_{high\text{-}T} + mQz + nH_2O.$$

In either case, no agent, whether it is fluid, mineral or otherwise, can stabilize the low-T zeolite on the high temperature side of the reaction. Among other considerations, neither heulandite nor stilbite nor chabazite can exist in the laumontite field. This means that the heulandite and chabazite had to have formed after laumonite in response to hydration and silicification at lower temperatures, effectively reversing the terminal reactions or initiating other reactions that produce the heulandite or chabazite in their respective fields. That the reactions did not proceed to completion, in the reverse sense, indicates that H_2O was intermittantly available. This may also explain the absence of stilbite. With regard to the zeolite minerals, the following paragenesis is envisioned:

(1) At the highest temperature laumonite was stable. Conditions did not reach the wairikite field.

(2) With declining temperature, in the heulandite field any free H_2O was consumed in the production of heulandite principally from plagioclase. Effectively all of the free H_2O was at least locally used up in the production of heulandite. Otherwise, there would be no relict plagioclase in the rock.

(3) At lower temperatures, in the stilbite field no free H2O was available for the production of stilbite.

(4) At still lower temperatures, chabazite formed in its field of stability in response to renewed, but limited, availability of H_2O.

7.2. Celadonite

The formation of the pseudomorphous minerals celadonite and calcite requires the involvement of a CO_2-H_2O fluid. In addition, the celadonite requires a source of K. It is assumed that the CO_2-H_2O fluid contained dissolved K in equilibrium with the orthoclase in the veins. The relevant reaction can involve de facto orthoclase. This is also necessary to account for the quartz in the pseudomorphs. The balanced reaction, involving the Mg-end member components, di and cel, may be written as follows:

$$cel^{Cel} + Qz + Cc = or^{Or} + di^{Aug} + CO_2 + H_2O,$$

expanded,

$$KMgAlSi_4O_{10}(OH)_2 + SiO_2 + CaCO_3 = KAlSi_3O_8 + CaMgSi_2O_6 + CO_2 + H_2O$$

The temperature at a given pressure for the equilibrium depends on the mole fraction of CO_2, $X(CO_2)$, in the aqueous phase. THERMOCALC results for the equilibrium are shown in **Figure 8** for three values of $X(CO_2)$, 0.00004, 0.0001 and 0.0004. Presumably the mole fraction of CO_2 in seawater (SW), $X(CO_2)$ = 0.00004, would be a lower limit. Values an order of magnitude higher than in seawater, $X(CO_2)$ = 0.0004, are permissable

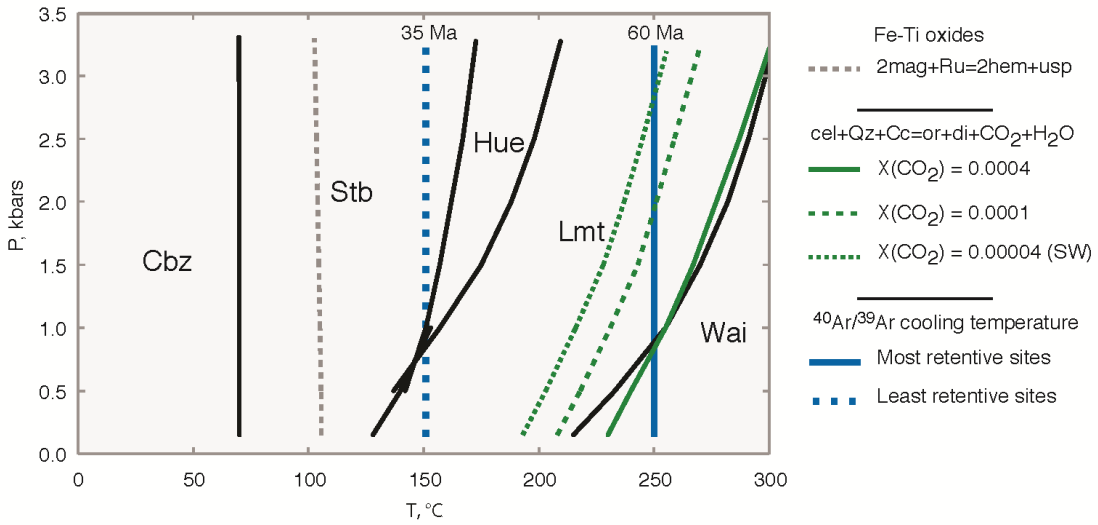

Figure 8. Phase relationships involving zeolites are shown as bold, black lines. Reactions involving stilbite (Stb), heulandite (Heu), laumontite (Lmt) and wairikite (Wai) are from Chu et al. (1987). The chabazite (Cbz) - stilbite reaction is from Chipera and Apps (2001). The temperature of the celadonite reaction (green lines), calculated by THERMOCALC, depends on the mole fraction of CO_2, $X(CO_2)$, in the fluid phase. $X(CO_2)$ in seawater (SW) is 0.00004. The equilibrium for Fe-Ti oxides (dashed gray line) was calculated by THERMOCALC. $^{40}Ar/^{39}Ar$ cooling temperatures (blue lines) and corresponding ages are from the Appendix 1.

within the field of stability for laumontite. Higher values for $X(CO_2)$ would involve temperatures in the field of stability for wairikite for pressures higher than ~1 kbar.

The $^{40}Ar/^{39}Ar$ age for the most retentive sites in feldspar in basement rock (Westphalia Schist) immediately beneath the unconformity at the base of the Wagwater Group indicates that temperature exceeded ~250°C for a time before 60 Ma (**Appendix 1**). The temperature is consistent with the THERMOCALC temperature for the celadonite equilibrium for $X(CO_2)$ between 0.0001 and 0.0004 in the range of pressure from ~1 kbar to ~2 kbar.

7.3. Fe-Ti oxides

Three equilibria involving components in the Fe-Ti oxides are of interest:

[1] $ilm^{Ilm} + mag^{Mag} = hem^{Ilm} + usp^{Mag}$, expanded,
$FeTiO_3 + Fe_3O_4 = Fe_2O_3 + Fe_2TiO_4$,

[2] $6\ ilm^{Ilm} + 2\ mag^{Mag} = 6\ usp^{Mag} + O_2$, expanded,
$6\ FeTiO_3 + 2\ Fe_3O_4 = 6\ Fe_2TiO_4 + O_2$, and

[3] $2\ mag^{Mag} + Ru = 2\ hem^{Ilm} + usp^{Mag}$, expanded,
$2\ Fe_3O_4 + TiO_2 = 2\ Fe_2O_3 + Fe_2TiO_4$

The first two equilibria [1, 2] are the basis for several formulations of a widely used thermo-oxybarometer (e.g., Spencer and Lindsey, 1981; Ghiorso and Sack, 1991; Sauerzapf et al., 2008). The compositions for titanomagnetite and ilmenite in this study (**Table 5**) are near, or just outside, the limits of applicability for these formulations. Nevertheless, estimates of temperature, by small extrapolation, are in the range from 750°C to 850°C, and estimates of $f(O_2)$ are in the range 10-12 bars to 10-11 bars. The temperatures are consistent with subsolidus equilibration, unrelated to diagenesis or burial metamorphism. Within limits defined by standard deviations of the chemical analyses (**Table 5**), the temperature is sensitive (+/-50°C) to variations in the compositions of the titanomagnetite and ilmenite.

Where rutile embays the titanomagnetite-ilmenite symplectite, it may be argued that the local equilibrium involves rutile, subject to reaction [3]. Like the first equilibrium [1], equilibrium [3] is independent of $f(O_2)$. THERMOCALC gives a temperature of ~105°C (**Figure 8**) for equilibrium [3], consistent with diagenesis or burial metamorphism. Within limits defined by the standard deviations of the chemical analyses (**Table 5**), the temperature for the third equilibrium [3] is also sensitive (+/-50°C) to the compositions of the titanomagnetite and ilmenite.

8. THERMAL HISTORY

A model for the thermal history of the oldest exposed strata of the Wagwater Group was developed using methods of multivariate analysis. **Figure 9** shows the favored solution. Control points are marked by the crosses (+) and are invariant in age. There are four invariant temperatures:

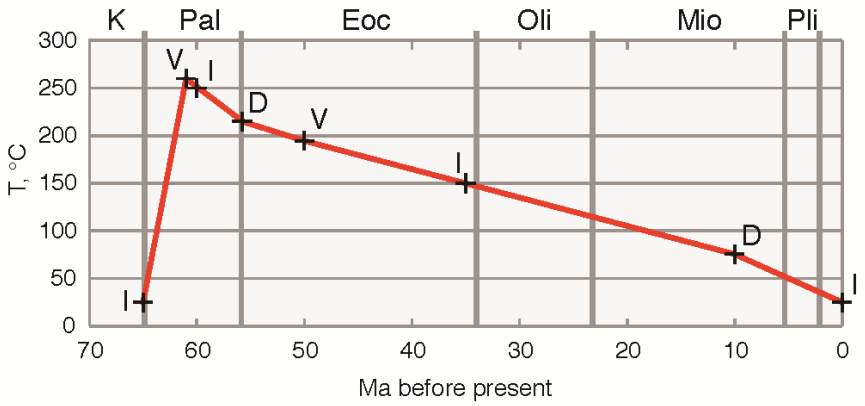

Figure 9. Thermal history of the lowest exposed strata of the Wagwater Group. In the multivariate model, the age at each control point (+) is invariant. At the control points marked "I" the temperature is invariant, at control points marked "V" the temperature is variable, and at the control points marked "D" the temperature is dependent. The first interval (65-61 Ma, I-V) relates to the lower Wagwater Formation, the second interval (61-56 Ma, V-I-D) relates to the upper Wagwater Formation, the third interval (56-50 Ma, D-V) relates to the Richmond Formation, the fourth interval (50-10 Ma, V-I-D relates to deposition of the limestone platform, and the fifth and final interval (10-0 Ma, D-I) relates to ongoing uplift.

(1) 25°C at 65 Ma,
(2) 25°C at 0 Ma (present),
(3) 250°C at 60 Ma (**Appendix 1**),
(4) 150°C at 35 Ma (**Appendix 1**).

There are two independently variable temperatures:

(5) 253-263°C at 61 Ma (favoured temperature, 258°C), highest temperature and commencement of cooling,

(6) 190-200°C at 50 Ma (favoured temperature, 195°C), beginning of limestone deposition.

Cooling had to have commenced prior to 60 Ma (**Appendix 1**; and see Abbott et al., 2013), during the deposition of the upper strata of the Wagwater Formation, well before the commencement of deposition of the Richmond Formation (56 Ma). Reasonable multivariate solutions that do not involve conditions in the wairikite field can be found in the temperature range from 253°C to 263°C at 61 Ma (5). The favoured temperature at 61 Ma (5) is 258°C. The highest temperature and commencement of cooling may have occured earlier than 61 Ma (5), but not much earlier without unrealistically high rates of heating in the first interval. Reasonable multivariate solutions can be found in the temperature range from 190°C to 200°C at 50 Ma (6). The favoured temperature at 50 Ma (6) is 195°C. Under the constraints of the analysis, there are two dependent temperatures:

(7) 218°C at 56 Ma (relates to 258°C at 61 Ma),
(8) 75°C at 10 Ma (relates to 195°C at 50 Ma).

By way of illustration, if the variable temperature at 61 Ma (5) is 263°C, the dependent temperature at 56 Ma (7) would be 198°C, maintaining a linear relationship between control points (3), (5) and (7). The same kind of relationship holds for control points (4), (6) and (8). Once cooling began, c. 61 Ma, the cooling rate decreases (slope becomes less negative), segment by segment, until 10 Ma. From 10 Ma to present the cooling rate increases (slope is more negative). The model does not tolerate much variation in the variable temperatures, (5) and (6), without creating on the profile intervals that are "flat," or intervals of unlikely cooling rate, or even more unlikely intervals of heating (positive slope).

9. P-T-TIME PATH

The P-T-time history (**Figure 10**; see also Abbott et al., 2013) of the lowest exposed strata of the Wagwater Formation combines the depth history (**Figure 4**) and the thermal history (**Figure 9**). The depth is expressed as equivalent pressure, 3 km ~ 1 kbar. Table 6 presents P-T slopes, rates of deposition or uplift, and rates of heating or cooling for each segment along the path. In the multivariate analysis, the only independently variable parameters are the the depth (pressure) and temperature at 61 Ma, and the temperature at 50 Ma. Variations in these parameters propogate through the depth history (**Figure 4**) and the thermal history (**Figure 9**). The favored path (**Figure 10**) satisfies the presumption that once cooling was underway (60 Ma) the rate of cooling decreased (became less negative in **Table 6**) until 10 Ma. Even small perturbations in the values for the three independent variables produce violations of this relationship. The P-T path involves "hot" burial and "cool" uplift (Abbott et al., 2011). In the context of the representation in **Figure 10**, the path is counter clockwise. This fundamental characteristic of the

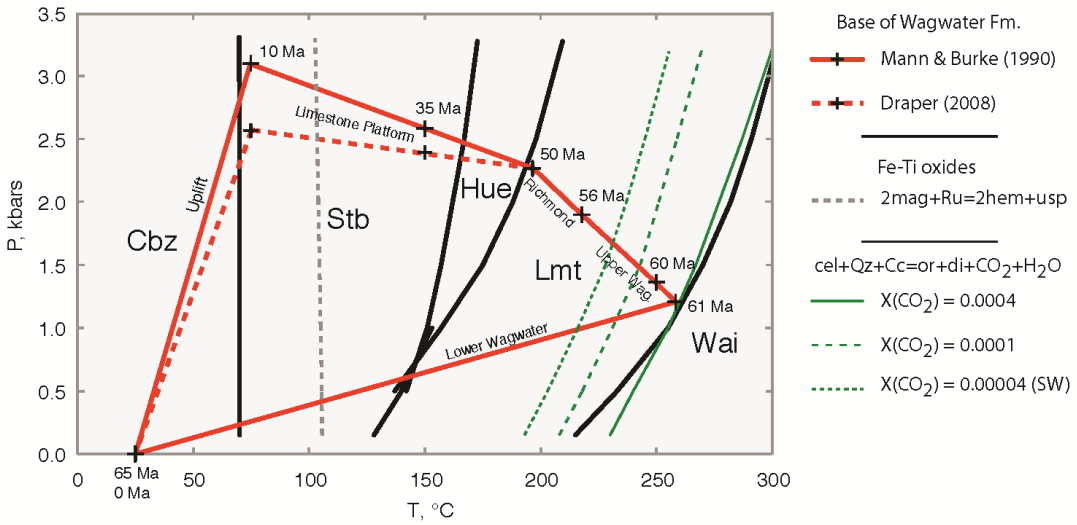

Figure 10. P-T history (red path) of the lowest exposed strata of the Wagwater Group. Depositional intervals are indicated by formation names. Phase relationships involving stilbite (Stb), heulandite (Heu), laumontite (Lmt) and wairikite (Wai) are from Chu et al. (1987). The chabazite (Cbz) - stilbite reaction is from Chipera and Apps (2001). The celadonite reactions (green lines) are from Figure 8. X(CO_2) in seawater (SW) is 0.00004. The equilibrium for Fe-Ti oxides is from Figure 8.

Table 6. Rates of uplift/subsidence, heating/cooling.

Time Interval		Subsidence & Uplift	Heating & Cooling	dP/dT
Myr		mm/yr	°C/Myr	kbars/°C
10-0	Uplift	0.93	-5	0.062
50-10	Limestone	-0.06	-3	-0.007
56-50	Richmond	-0.20	-4	-0.017
61-56	Upper Wagwater	-0.42	-8	-0.018
65-61	Lower Wagwater	-0.88	58	0.005

path is not altered by any reasonable variation in the three independent variables.

10. Discussion and Conclusions

Late, low-grade metamorphism has been described both in the basement rock beneath the Wagwater Group (Draper, 1987; Abbott et al., 1996) and in the Richmond Formation of the upper part Wagwater Group (Wright and Dickinson, 1972). Evidence for low grade metamorphism in the Richmond Formation (Wright and Dickinson, 1972) and undifferentiated Richmond Formation in the eastern part of the Wagwater basin (Rajkumar, 2011) is principally in the form of chlorite, albitization of plagioclase, and illite. K-Ar ages on biotite (Lewis et al., 1973) and $^{40}Ar/^{39}Ar$ ages (**Appendix 1**) require a Paleocene-Eocene thermal event affecting the basement rocks. By all indications this thermal event was widespread in the Wagwater Basin, with manifestations of the highest grade in the lowest strata of the Wagwater Group. The P-T path for rocks near the base of the Wagwater Group (**Figure 10**) consists of three distinct parts: (1) rapid burial and heating (lower Wagwater Fm.), (2) continued burial, but with cooling (upper Wagwater Fm., Richmond Fm., limestone platform), and (3) rapid uplift and cooling. While heating was rapid, cooling was protracted over at least 50 Myr before uplift. These attributes argue for a regional event of burial metamorphism, rather than one or more brief, episodic events, that might otherwise be relegated to localized, "hydrothermal alteration."

The highest temperature metamorphic minerals (celadonite, laumontite, chlorite) are consistent with upper zeolite facies (Coombs et al., 1959; Miyashiro and Shido, 1970; Miyashiro, 1973; Utada, 2001). Retrograde heulandite and chabazite are consistent with lower grade zeolite facies. The preservation of the laumonite, heulandite and primary volcanic plagioclase indicate that H_2O was intermittently available, but this limited availability was controlled in large part by the prograde and retrograde mineral reactions. The formation of chabazite requires a late influx of H_2O during uplift. The required H_2O may have been provided by groundwater at shallow depths. Circulation of groundwater may also have been responsible for the accelerated rate of cooling (**Table 6**) during final uplift.

An important conclusion is that the thermal peak for the oldest exposed strata of the Wagwater Formation may well have occurred during the deposition of younger strata of the same formation. K-Ar ages for biotite (50-54 Ma, Lewis et al., 1973)

and $^{40}Ar/^{39}Ar$ ages (60 Ma, Appendix) come from basement Westphalia schist in the eastern part of the basin, where the schist is overlain nonconformably by undifferentiated Richmond Formation. This suggests that the undifferentiated Richmond Formation of the eastern part of the Wagwater basin is actually a distal facies of the lower Wagwater Formation, as implied by Mann and Burke (1990) and Draper (2008). As such, undifferentiated Richmond Formation in the eastern part of the basin may be as old as (Robinson, 1997), or even older than (Mann and Burke, 1990; Draper, 2008), the oldest exposed Wagwater strata in the western part of the basin. This makes intuitive sense, assuming the inferred nonconformity at the base of the Wagwater Formation in the western part of the basin and the nonconformity at the base of the undifferentiated Richmond Formation in the eastern part of the basin are related to the same Early Paleocene erosional surface.

Acknowledgements. *We appreciate the time and patience of Dr. Guichuan Hou, director of the College of Arts and Sciences Microscope Facility, Appalachian State University. We are grateful for the helpful comments of the reviewer and the editor. We also thank Dave West for permitting us to present new $^{40}Ar/^{39}Ar$ data on Westphalia Schist (**Appendix 1**).*

REFERENCES

Abbott, R.N., Jr. and Bandy, B.R. 2008. Amphibolite and Blueschist-Greenschist Facies Metamorphism, Blue Mountain Inlier, Eastern Jamaica. In: **Donovan, S.K. (Ed.)**, *Geological crustal and biotic evolution of the Caribbean Plate: A tribute to T. A. Jackson. Geological Journal*, **43**, 525-541.

Abbott, R.N., Jr., Bandy, B.R., Jackson, T.A. and Scott, P.W. 2003. Blueschist-greenschist transition in the Mt. Hibernia Schist, Union Hill, Jamaica. *International Geology Review*, **45**, 1-15.

Abbott, R.N., Jr., Bandy, B.R. and Rajkumar, A. 2013. Upper zeolite facies burial metamorphism in Paleocene-Eocene redbeds of the Wagwater Group, eastern Jamaica. *Geological Society of America, Abstract with Program, Southeastern Section, San Juan*.

Abbott, R.N., Jr., Jackson, T.A. and McSween, H.Y., Jr. 1996. Metamorphic conditions in the Westphalia Schists of the Blue Mountain Inlier, Jamaica: tectonic implications. *International Geology Review*, **38**, 1143-1154.

Abbott, R.N., Jr., West, D.P., Jr. and Bandy, B.R. 2011. Thermotectonic history of metamorphic rocks in the Blue Mountain Inlier, Jamaica. *19th Caribbean Geological Conference, Guadeloupe. Program and Abstracts*, 56-57.

Chipera, S.J. and Apps, J.A. 2001. Geochemical stability of natural zeolites. In: **D.L. Bish and D.W. Ming (Eds.)**, *Natural Zeolite: Occurrence, properties, applications. Reviews in Mineralogy and Geochemistry*, **45**, 116-161.

Cho, M., Maruyama, S. and Liou, J.G. 1987. An experimental investigation of heulandite-laumontite equilibrium at 1000 to 2000 bar Pfluid. *Contributions to Mineralogy and Petrology*, **97**, 43-50.

CNMMN (Commission on New Minerals and Mineral Names of the International Mineralogical Association) 1997. Recommended nomenclature for zeolite minerals: Report of the subcommittee on zeolites of the International Mineralogical Association, Commission on new Minerals and mineral names. *Canadan Mineralogist*, **35**, 1571-1606.

CNMMN (Commission on New Minerals and Mineral Names of the International Mineralogical Association) 1998. Nomenclature of the micas. *Canadian Mineralogist*, **36**, 905-912.

Coombs, D.S., Ellis, A.J., Fyfe, W.S. and Taylor. 1959. The zeolite facies, with comments on the interpretation of hydrothermal synthesis. *Geochimica et Cosmochimica Acta*, **17**, 53-107.

DeMets, C. and Wiggins-Grandison, M. 2007. Deformation of Jamaica anad motion of the Gonave microplate from GPS and seismic data. *Geophysical Journal International*, **168**, 362-378.

Deer, W.A., Howie, R.A. and Zussman, J. 1966. *An Introduction to the Rock Forming Minerals*. Longman Group Ltd. England, 528 pp.

Draper, G. 1987. Petrology of the metamorphic rocks of the Blue Mountains, Jamaica. In: **Ahmad, R. (Ed.)**, *Proceedings of a Workshop on the Status of Jamaican Geology. Geological Society of Jamaica Speciaal Issue*, 120-150.

Draper, G. 1998. Geological and tectonic evolution of Jamaica. *Contributions to Geology, University of the West Indies, Mona*, **#3**, 3-9.

Draper, G. 2008. Some speculations on the Paleogene and Neogene tectonics of Jamaica. *Geological Journal*, **43**, 563-572.

Ghiorso, M.S. and Sack, R.O. 1991. Fe-Ti oxide geothermometry: thermodynamic formulation and estimation of intensive variables in silicic magmas. *Contributions to Mineralogy and Petrology*, **108**, 485-510.

Gradstein, F.M., Ogg, J.G., Schmitz, M.D. and Ogg, G. 2012. *The Geologic Time Scale 2012*, Elsevier, Boston, 1176 pp.

Holland, T.J.B. and Powell R. 1998. An internally consistent thermodynamic data set for phases of petrologic interest. *Journal of Metamorphic Geology*, **16**, 309-343.

Holland, T.J.B. and Powell, R. 2000. *AX, Mineral activity calculation for thermobarometry. Cambridge University, Cambridge, computer program AX2* (v. 2.2). web site: https://www.esc.cam.ac.uk/research/research-groups/holland/ax

Kretz, R. 1983. Symbols for rock-forming minerals.

American Mineralogist, **68**, 277–279.

Lewis, J.F., Harper,C.T., Kemp, A.W. and Stipp, J.J. 1973. Potassium-Argon retention ages of some Cretaceous rocks from Jamaica. *Geological Society of America Bulletin*, **84**, 335-340.

Lovera, O.M., Grove M. and Harrison, T.M. 2002. Systematic analysis of K-feldspar $^{40}Ar/^{39}Ar$ step heating results II: Relevance of laboratory argon diffusion properties to nature. *Geochimica et Cosmochimica Acta*, **67**, 1237-1255.

Mann, P. and Burke, K. 1990. Tranverse intra-arc rifting: Paleogene Wagwater Belt, Jamaica. *Marine and Petroleum Geology*, **7**, 410-427.

Mann, P., DeMets, C. and Wiggins-Grandison, M. 2007. Toward a better understanding of the Late Neogene strike-slip restraining bend in Jamaica: Geodetic, geologic, and seismic constraints. In: **W.D. Cunningham and P. Mann (Eds.)**, *Tectonics of Strike-slip Restraining and releasing Bends. Geological Society of London Special Issue*, **290**, 239-253.

Mann, P., Draper, G. and Burke, K. 1985. Neotectonics of a strike-slip restraining bend system, Jamaica. In: **K. Biddle and N. Christie-Blick (Eds.)**, *Strike-slip deformation, basin formation, and sedimentation. SEPM Special Issue*, **37**, 211-226.

McDougall, I. and Harrison, T.M. 1999. *Geochronology and thermochronology by the $^{40}Ar/^{39}Ar$ method*. Oxford University Press, New York, Second Edition, 269 pp.

Mitchell, S.F. 2003. Sedimentary and tectonic evolution of central Jamaica. In: **C. Bartolini, R.T. Buffler and J.F. Blickwede (Eds.)**, *The Circum-Gulf of Mexico and the Caribbean: hydrocarbon habitats, basin formation, and plate tectonics. American Association of Petroleum Geologists Memoir*, **79**, 605-623.

Mitchell, S.F. 2006. Timing and implications of Late Cretaceous tectonic and sedimentary events in Jamaica. *Geologica Acta*, **4**, 171-178.

Mitchell, S.F. 2013. Stratigraphy of the White Limestone of Jamaica. *Bulletin de la Société Géologique de France*, **184**, 111-118.

Miyashiro, A. 1973. *Metamorphism and Metamorphic Belts*. George Allen & Unwin, Ltd., London. 492 pp.

Miyashiro, A. and Shido, F. 1970. Progressive metamorpism in zeolite assemblages. *Lithos*, **3**, 251-260.

Pickerill, R.K., Donovan, S.K. and Dixon, H.L. 1992. The Richmond Formation of eastern Jamaica revisited - Further ichnological observations. *Carribean Journal of Science*, **28**, 89-98.

Powell, R. 2005. *THERMOCALC*, (v. tc325). web site: http://www.esc.cam.ac.uk/research/research-groups/holland/thermocalc

Powell, R., Holland, T.J.B. and Worley, B.A. 1998. Calculating phase diagrams involving solutions via non-linear equations, with examples using THERMOCALC. *Journal of Metamorphic Geology*, **16**, 577-588.

Rajkumar, A. 2011. *Pressure-Temperature Analysis of the Richmond Formation, Jamaica.* B.A. honors thesis, Department of Geology, Appalachian Sate University, North Carolina. 52 pp.

Robinson, E. 1994. Jamaica. In: **S.K. Donovan and T.E. Jackson (Eds.)**, *Caribbean geology, an introduction*. The University of the West Indies Publishers' Association, Kingston, 111-127.

Robinson, E. 1997. Paleocene fossils from the White Limestone Group in eastern Jamaica. *Journal of the Geological Society of Jamaica*, **32**, 43-46.

Sauerzapf, U., Lattard, D., Burchard, M. and Engelmann, R. 2008. The titanomagnetite-ilmanite equilibrium: New experimental data and thermo-oxybarometric applications to the crystallization of basic and intermediate rocks. *Journal of Petrology*, **49**, 1161-1185.

Spear, F.S. 1983. *Metamorphic Phase Equilibria and Pressure-Temperature-Time Paths*. Mineralogical Society of America Monograph, 799 pp.

Spencer, K.J. and Lindsey, D.H. 1981. A solution model for coexisting iron-titanium oxides. *American Mineralogist*, **66**, 1189-1201.

Steiger, R.H. and Jäger, E. 1977. Subcommission on geochronology, convention on the use of decay constants in geo- and cosmochronology. *Earth and Planetary Science Letters*, **36**, 359-362.

Utada, M. 2001. Zeolites in burial diagenesis and low-grade metamorphic rocks. In: **D.L. Bish and D. W. Ming (Eds.)**, *Natural Zeolite: Occurrence, properties, applications. Reviews in Mineralogy and Geochemistry*, **45**, 277-304.

Whitney, D.L. and Evans, B.W. 2010. Abbreviations for names of rock-forming minerals. *American Mineralogist*, **95**, 185-187.

Wright, R.M. and Dickinson, W.R. 1972. Provenance of Eocene volcanic sandstones in eastern Jamaica – a preliminary Note. *Caribbean Journal of Science*, **12**, 107-113.

Accepted 14th July 2013

Appendix 1: $^{40}Ar/^{39}Ar$ Geochronology

In a personal communication (West, D.P., Jr., Abbott, R.N., Jr., Bandy, B.R. and Kunk, M.J.) new $^{40}Ar/^{39}Ar$ data were made available on two samples of Mt. Hibernia Schist and three samples of Westphalia Schist. The following summarizes the $^{40}Ar/^{39}Ar$ data on Westphalia Schist, specifically relevant to this paper. The data pertain to whole-rock analyses for one sample (JAM-09-01), and K-feldspar + quartz separated from two samples (JAM-09-04, JAM-09-06). The samples are from the main body of Westphalia Schist. Two of the rocks, JAM09-01 (fine-grained amphibolite) and JAM-09-4 (fine-grained biotite chlorite schist), were collected at Mahogany Vale (N18°01'19.6", W76°37'55.4" and N18°01'20.0", W76°37'57.0", respectively), and one of the rocks, JAM-09-6 (fine-grained amphibolite),

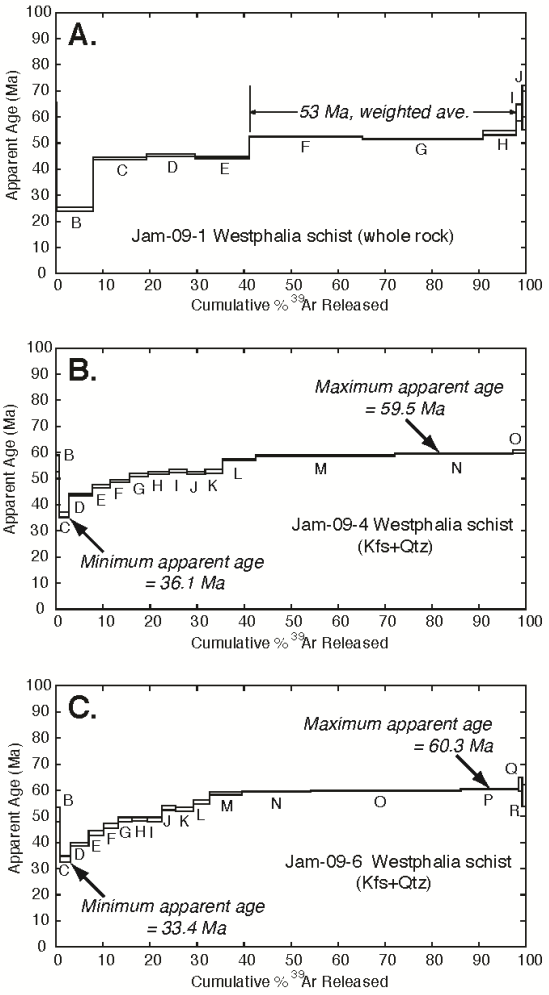

Figure 11. Ar-release data for Westphalia Schist (West et al., personal communication).

was collected near the village of Westphalia (N18°03'26.4", W76°39'1.1"). The sample location for JAM-09-06 is approximately 4 km away from the the sample locations for JAM-09-01 and JAM-09-04. The samples were analyzed by $^{40}Ar/^{39}Ar$ incremental heating (10 heating steps for JAM-09-01; 14 heating steps for JAM-09-04; 17 heating steps for JAM-09-06). The analyses were performed at the U.S. Geological Survey argon dating lab in Reston, Virginia (Michael Kunk). The argon-release spectra are presented in **Figure 11**. Ar-release data are in **Table 7**.

The age spectrum for the whole-rock analyses (Figure 11 A, JAM-09-01) is highly discordant. The apparent ages increase systematically from low-temperature extractions to older ages in the mid- to high-temperature steps. The apparent ages for 90% of the ^{39}Ar released in 6 of 10 steps (steps, C, D, E, F, G, H) range from 44 to 54 Ma, with a weighted average of 53 Ma for 56% of the ^{39}Ar released (steps F, G, H).

The two K-feldspar + quartz samples yield remarkably similar results (**Figure 11B, C**). After initial, small-yield heating steps (steps A, B), each sample displays low-temperature apparent ages in the range 33-36 Ma (step C). The low apparent ages reflect either degassing of lower temperature argon-retention sites or closure at a later time than the higher temperature, more retentive sites. Both of these proceses would be associated with a closure temperature of approximately 150°C (McDougall and Harrison, 1999; Lovera et al., 2002). In both samples, apparent ages then systematically step up to maximum ages of approximately 60 Ma. These maximum apparent ages reflect a minimum age of degassing of the most retentive sites in K-feldspar and correspond to a minimum closure temperature of approximately 250°C (McDougall and Harrison, 1999; Lovera et al., 2002). In their analysis of two models of Multidiffusion Domain (MDD) theory, Lovera et al. (2002) show that: *"As in the case of model A, the calculated age spectrum [for model B] remains largely unaffected when recrystallization occurs at temperatures in excess of 250°C. This is because even when the four smallest domains comprise more than 60% of the sample, they are completely open to argon loss at temperatures beyond 250°C."*

A simple explanation for this kind of Ar-release spectrum can be found in Spear (1983, pp. 721-724, figure 20-5B).

Table 7. Ar-release data for Westphalia Schist[a]

Jam-09-1 ***Whole rock*** *: J = 0.009413 ± 0.50%, wt. = 0.00387 g*									
Step	**Temp.**	**^{39}Ar**	**Radiogenic Yield**	**$^{39}Ar_k$**	**$^{40}Ar^*/^{39}Ar_k$**	**K/Ca**	**K/Cl**	**Age**	**Error**
	(C)	*(% of total)*	*(%)*	*(moles)*				*(Ma)*	*(Ma)*
A	550	0.3	3.0	5.28E-17	2.779	0.92	19	46.59	18.66
B	750	7.6	27.2	1.24E-15	1.457	1.09	57	24.57	0.79
C	850	11.4	82.8	1.87E-15	2.618	1.10	104	43.93	0.46
D	950	10.3	78.7	1.69E-15	2.696	0.60	181	45.22	0.50
E	1050	11.6	78.3	1.89E-15	2.644	0.38	291	44.34	0.46
F	1150	23.9	89.9	3.90E-15	3.133	0.55	337	52.44	0.23
G	1250	25.9	79.3	4.22E-15	3.068	0.53	32	51.37	0.23
H	1300	6.9	79.5	1.13E-15	3.212	0.20	35	53.73	0.75
I	1350	1.4	68.5	2.35E-16	3.689	0.10	28	61.58	3.24
J	1450	0.6	49.9	9.61E-17	3.800	0.06	15	63.40	8.37
Total Gas			77.6	1.63E-14	2.844	0.60	161	47.70	

JAM-09-4 ***K-Spar*** *Conc 121KD54; J = 0.009409 ± 0.50%, wt. = 0.00136 g*									
Step	**Temp.**	**^{39}Ar**	**Radiogenic Yield**	**$^{39}Ar_k$**	**$^{40}Ar^*/^{39}Ar_k$**	**K/Ca**	**K/Cl**	**Age**	**Error**
	(C)	*(% of total)*	*(%)*	*(moles)*				*(Ma)*	*(Ma)*
B	700	0.7	51.9	3.792E-16	3.333	7.4	51	55.7	2.97
C	800	2.1	88.9	1.174E-15	2.149	27.7	137	36.1	0.99
D	900	4.9	93.9	2.688E-15	2.598	52.3	282	43.6	0.43
E	950	3.9	93.2	2.168E-15	2.798	156.5	515	46.9	0.53
F	1000	4.0	94.5	2.171E-15	2.933	113.4	676	49.1	0.52
G	1050	4.0	97.0	2.226E-15	3.061	117.9	855	51.2	0.53
H	1100	4.4	97.1	2.447E-15	3.108	144.5	800	52.0	0.50
I	1150	3.8	97.3	2.066E-15	3.151	121.4	617	52.7	0.54
J	1200	3.9	95.8	2.141E-15	3.118	43.3	474	52.2	0.53
K	1250	3.6	77.2	1.981E-15	3.146	89.2	36	52.6	0.60
L	1300	7.3	91.3	4.013E-15	3.414	76.1	99	57.0	0.36
M	1350	29.5	97.5	1.613E-14	3.516	200.8	361	58.7	0.09
N	1450	25.2	97.3	1.374E-14	3.563	189.8	503	59.5	0.10
O	1550	2.7	92.7	1.470E-15	3.600	885.0	102	60.1	0.77
Total Gas			95.1	5.480E-14	3.318	170.9	420	55.4	

JAM-09-6 ***K-Spar*** *Conc 123KD54; J = 0.009393 ± 0.50%, wt. = 0.00105 g*									
Step	**Temp.**	**^{39}Ar**	**Radiogenic Yield**	**$^{39}Ar_k$**	**$^{40}Ar^*/^{39}Ar_k$**	**K/Ca**	**K/Cl**	**Age**	**Error**
	(C)	*(% of total)*	*(%)*	*(moles)*				*(Ma)*	*(Ma)*
B	700	0.9	42.8	3.380E-16	3.020	5.1	40	50.5	2.88
C	800	2.3	78.5	8.819E-16	1.991	13.5	83	33.4	1.08
D	900	3.8	88.8	1.482E-15	2.343	75.2	159	39.3	0.67
E	950	3.3	86.6	1.296E-15	2.597	46.6	291	43.5	0.78
F	1000	3.2	88.3	1.225E-15	2.759	40.1	433	46.2	0.77
G	1050	2.9	91.8	1.116E-15	2.906	99.0	599	48.6	0.89
H	1100	3.2	91.4	1.253E-15	2.919	37.9	485	48.8	0.75
I	1150	3.1	90.6	1.218E-15	2.904	33.6	383	48.6	0.77
J	1200	2.9	97.8	1.118E-15	3.179	***	258	53.1	0.95
K	1250	3.9	68.6	1.537E-15	3.149	41.0	20	52.6	0.68
L	1275	3.5	87.8	1.372E-15	3.319	209.2	37	55.4	0.68
M	1300	6.9	95.4	2.673E-15	3.514	147.1	149	58.6	0.39
N	1325	14.7	97.5	5.680E-15	3.553	175.7	210	59.2	0.18
O	1350	31.9	97.8	1.247E-14	3.592	194.9	294	59.9	0.10
P	1400	12.2	97.1	4.777E-15	3.621	144.7	327	60.3	0.21
Q	1450	0.9	90.8	3.601E-16	3.734	19.0	132	62.2	2.58
R	1550	0.6	79.0	2.291E-16	3.461	21.8	118	57.7	4.09
Total Gas			93.3	3.902E-14	3.335	140.0	262	55.7	

[a]Data from Dave West, Middlebury College, Vermont, USA; Michael Kunk, US Geological Survey, Reston, Virginia, USA